Journal of Molecular Structure 1030 (2012) 26–39

Contents lists available at SciVerse ScienceDirect

Journal of Molecular Structure

journal homepage: www.elsevier.com/locate/molstruc

# Synthesis, spectroscopic, thermal and antimicrobial investigations of charge-transfer complexes formed from the drug procaine hydrochloride with quinol, picric acid and TCNQ

Abdel Majid A. Adam *

*Department of Chemistry, Faculty of Science, Taif University, Al-Hawiah, P.O. Box 888, Zip Code 21974 Taif, Saudi Arabia*

## HIGHLIGHTS

- Three new CT-complexes of procaine hydrochloride drug are characterized.
- Various spectroscopic and thermal analyses are used.
- XRD confirmed that the obtained complexes located within nanoscale range.

## ARTICLE INFO

*Article history:*
Received 6 June 2012
Received in revised form 7 July 2012
Accepted 10 July 2012
Available online 23 July 2012

*Keywords:*
Procaine hydrochloride
Proton-transfer
Thermal analysis
Antimicrobial activity

## ABSTRACT

Intermolecular charge-transfer or proton-transfer complexes between the drug procaine hydrochloride (PC-HCl) as a donor and quinol (QL), picric acid (PA) or 7,7′,8,8′-tetracyanoquinodimethane (TCNQ) as a π-acceptor have been synthesized and spectroscopically studied in methanol at room temperature. Based on elemental analyses and photometric titrations, the stoichiometry of the complexes (donor:acceptor molar ratios) was determined to be 1:1 for all three complexes. The formation constant ($K_{CT}$), molar extinction coefficient ($\varepsilon_{CT}$) and other spectroscopic data have been determined using the Benesi–Hildebrand method and its modifications. The newly synthesized CT complexes have been characterized via elemental analysis, IR, Raman, $^1$H NMR, and electronic absorption spectroscopy. The morphological features of these complexes were investigated using scanning electron microscopy (SEM), and the sharp, well-defined Bragg reflections at specific 2$\theta$ angles have been identified from the powder X-ray diffraction patterns. Thermogravimetric analyses (TGAs) and kinetic thermodynamic parameters were also used to investigate the thermal stability of the synthesized solid CT complexes. Finally, the CT complexes were screened for their antibacterial and antifungal activities against various bacterial and fungal strains, and only the complex obtained using picric acid exhibited moderate antibacterial activity against all of the tested strains.



## 1. Introduction

Procaine hydrochloride (PC-HCl; 2-(diethylamino)ethyl-4-aminobenzoate hydrochloride, Formula I) is a synthetic local anesthetic drug of the amino ester family that produces a reversible loss of sensation by diminishing the conduction of sensory nerve impulses [1,2]. Procaine has long been employed as a pharmacological agent in the life sciences and in clinical therapeutic studies. This drug is primarily used to reduce pain from the intramuscular injection of penicillin, and it is also used in dentistry [3,4]. Procaine was first synthesized in 1905 under the trade name Novocaine (or Novocain) as the first injectable synthetic local anesthetic. Before the discovery of procaine, cocaine was the most commonly used local anesthetic. Furthermore, ever since Koller used cocaine to anesthetize a cornea in 1844, local anesthetics have been under continuous development. Procaine has low toxicity and low stimulus and is not toxic to the central nervous system [5].

Charge-transfer complexation is of great importance in chemical reactions, including addition, substitution, condensation [6,7], biochemical and bioelectrochemical energy-transfer processes [8], biological systems [9], and drug–receptor binding mechanisms. For example, drug action, enzyme catalysis, ion transfers through lipophilic membranes [10], and certain π-acceptors have been successfully utilized in the pharmaceutical analysis of some drugs in pure form or in pharmaceutical preparations [11–17]. Furthermore, charge-transfer complexation is also of great importance in many applications and fields, such as in non-linear optical materials, electrically conductive materials [18–21], second-order non-linear optical activity [22], microemulsions [23], surface

* Tel.: +966 502099808.
*E-mail address:* majidadam@yahoo.com

0022-2860/$ - see front matter © 2012 Elsevier B.V. All rights reserved.
http://dx.doi.org/10.1016/j.molstruc.2012.07.017

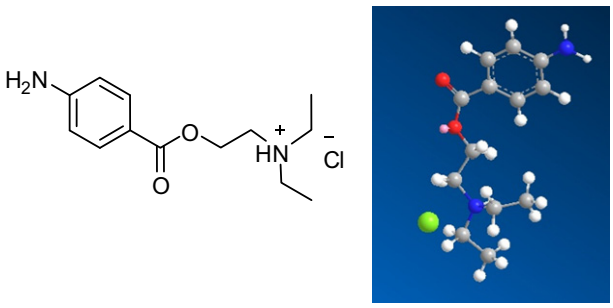


**Formula I.** Molecular structure of procaine hydrochloride.

chemistry [23], photocatalysts [24], dendrimers [25], solar energy storage [26], organic semiconductors [27], and the investigation of redox processes [28]. Charge-transfer complexes that use organic species are intensively studied because of their special type of interaction, which is accompanied by the transfer of an electron from the donor to the acceptor [29,30]. In addition, the protonation of the donor from acidic acceptors is a route for the formation of ion-pair adducts [31–33].

This paper describes the formation of CT complexes between procaine hydrochloride (PC-HCl) as a donor and quinol (benzene-1,4-diol, QL), picric acid (2,4,6-trinitrophenol, PA), or 7,7′,8,8′-tetracyanoquinodimethane (TCNQ). The nature and structure of the final products both in solution and in the solid phase have been characterized using elemental analysis, infrared (IR), Raman, $^1$H NMR and electronic absorption spectroscopy, powder X-ray diffraction and scanning electron microscopy (SEM) to interpret the behavior of the interactions. The thermal behavior of the obtained complexes and the kinetic and thermodynamic parameters ($E^*$, $A$, $\Delta S^*$, $\Delta H^*$ and $\Delta G^*$) have also been investigated. Finally, the antimicrobial activity of the PC-HCl complexes was tested against various bacterial and fungal strains.

## 2. Experimental

### 2.1. Materials

Procaine hydrochloride (PC-HCl) (MF = $C_{13}H_{21}N_2O_2Cl$) and π-acceptors of quinol (QL), picric acid (PA) and 7,7′,8,8′-tetracyanoquinodimethane (TCNQ) were of analytical reagent grade (Merck) and were used without further purification.

### 2.2. Synthesis of the solid CT complexes

The solid CT complexes of PC-HCl with QL, PA, and TCNQ were synthesized by mixing 1 mmol of PC-HCl in methanol (10 ml) with 1 mmol of each acceptor in the same solvent. The mixtures were stirred at room temperature for 15 min, which resulted in the precipitation of the solid CT complexes. The solid precipitates were filtered, washed several times with methanol, and then dried under vacuum over anhydrous calcium chloride.

### 2.3. Photometric titration measurements

Photometric titration measurements were performed for the reactions of the donor with QL, PA, and TCNQ against methanol as a blank, at wavelengths of 296, 355, and 299 nm, respectively. A 0.25, 0.50, 0.75, 1.00, 1.50, 2.0, 2.50, 3.00, 3.50 or 4.00 ml aliquot of a standard solution ($5.0 \times 10^{-4}$ M) of the appropriate acceptor in MeOH was added to 1.00 ml of $5.0 \times 10^{-4}$ M PC-HCl, which was also dissolved in MeOH. The total volume of the mixture was 5 ml. The concentration of PC-HCl ($C_d$) in the reaction mixture was maintained at $5.0 \times 10^{-4}$ M, whereas the concentration of the π-acceptors ($C_a$) changed over a wide range of concentrations ($0.25 \times 10^{-4}$–$4.00 \times 10^{-4}$ M) to produce solutions with an acceptor molar reaction that varied from 4:1 to 1:4. The stoichiometry of the molecular CT complexes was determined from the determination of the conventional spectrophotometric molar ratio according to the known methods [34] using a plot of the absorbance of each CT complex as a function of the $C_d$:$C_a$ ratio. Modified Benesi–Hildebrand plots were constructed [35,36] to allow calculations of the formation constant, $K_{CT}$, and the absorptivity, $\varepsilon_{CT}$, values for each CT complex in this study.

### 2.4. Instrumentation

#### 2.4.1. Elemental analyses

The elemental analyses of the carbon and hydrogen contents were performed by the microanalytical unit at Cairo University, Egypt, using a Perkin–Elmer CHN 2400 (USA).

#### 2.4.2. Electronic spectra

The electronic absorption spectra of the methanol solutions of the donor, acceptors and resulting CT complexes were recorded in wavelength range of 200–800 nm using a Perkin–Elmer Lambda 25 UV/Vis double-beam spectrophotometer at Taif University, Saudi Arabia. The instrument was equipped with a quartz cell with a 1.0 cm path length.

#### 2.4.3. Infrared and Raman spectra

The mid-infrared (IR) spectra (KBr discs) within the range of 4000–400 cm$^{-1}$ for the solid CT complexes were recorded on a Shimadzu FT-IR spectrophotometer with 30 scans at 2 cm$^{-1}$ resolution. The Raman laser spectra of the samples were measured on a Bruker FT-Raman spectrophotometer at Taif University, Saudi Arabia; the spectrophotometer was equipped with a 50 mW laser.

#### 2.4.4. $^1$H NMR spectra

$^1$H NMR spectra were collected by the Analytical Center at King Abdul Aziz University, Saudi Arabia, on a Bruker DRX-250 spectrometer operated at 250.13 MHz with a dual 5 mm probe head. The measurements were performed at ambient temperature using DMSO-$d_6$ (dimethylsulfoxide, $d_6$) as a solvent and TMS (tetramethylsilane) as an internal reference. The $^1$H NMR data are expressed in parts per million (ppm) and are internally referenced to the residual proton impurity in the DMSO solvent.

#### 2.4.5. Thermal analysis

Thermogravimetric analysis (TGA) was performed under air atmosphere between room temperature and 800 °C at a heating rate of 10 °C/min using a Shimadzu TGA–50H thermal analyzer at the Central Lab at Ain Shams University, Egypt.

#### 2.4.6. X-ray diffraction patterns

The X-ray diffraction patterns for the obtained CT complexes were collected on a PANalytical X'Pert PRO X-ray powder diffractometer at the Central Lab at Ain Shams University, Egypt. The instrument equipped with a Ge(III) monochromator before the sample and a Cu K$\alpha_1$ X-ray source with a wavelength of 0.154056 nm was used.

#### 2.4.7. SEM and EDX detection

Scanning electron microscopy (SEM) images and energy-dispersive X-ray spectroscopy (EDX) patterns were collected on a Jeol JSM-6390 instrument at Taif University, Saudi Arabia. The instrument was operated at an accelerating voltage of 20 kV.

### 2.5. Antimicrobial investigation

The antimicrobial activities of the PC-HCl CT complexes and the pure solvent were determined using a modified Bauer–Kirby disc diffusion method [37] against different Gram (+) and Gram (−) bacteria species: *Staphylococcus aureus*, *Bacillus subtilis*, *Escherichia coli* and *Pseudomonas aeuroginosa*. Antifungal screening was studied against two species: *Aspergillus flavus* and *Candida albicans*. The microanalysis unit at Cairo University, Egypt performed the investigations. For these investigations, 100 μl of the test bacteria/fungi were grown in 10 ml of fresh media until they reached a count of approximately 108 cells/ml for bacteria or 105 cells/ml for fungi [38]. One hundred microliters of the microbial suspension was spread onto agar plates. The nutrient ager medium for the antibacterial tests consisted of 0.5% peptone, 0.1% beef extract, 0.2% yeast extract, 0.5% NaCl and 1.5% agar–agar. The medium for the antifungal tests consisted of 3% sucrose, 0.3% $NaNO_3$, 0.1% $K_2HPO_4$, 0.05% KCl, 0.001% $FeSO_4$ and 2% agar–agar [39]. Isolated colonies of each organism that might be playing a pathogenic role were selected from the primary agar plates and tested for susceptibility. The disc diffusion method for the filamentous fungi was tested using the developed standard method M38-A [40], whereas the disc diffusion method for yeast was tested using the developed standard method M44-P [41]. Plates inoculated with filamentous fungi, bacteria or yeast were incubated at 25 °C, 35–37 °C or 30 °C, respectively. After the plates were incubated for 48 h, the inhibition (sterile) zone diameters (including disc) were measured using slipping calipers from the National Committee for Clinical Laboratory Standards (NCCLS, 1993) [42] and are expressed in mm. Standard discs of tetracycline (antibacterial agent) and Amphotericin B (antifungal agent) served as positive controls for antimicrobial activity, whereas filter discs impregnated with 10 μl of DMSO solvent were used as a negative control. An inhibition zone diameter greater than 8 mm indicates that the tested compounds are active against some of the bacteria and fungi under investigation. The concentration of each solution was $1.0 \times 10^{-3}$ mol $dm^{-3}$. Commercial DMSO was used to dissolve the tested samples.

## 3. Results and discussion

### 3.1. Elemental analysis

Elemental analyses (C, H, and N) of the PC-HCl CT complexes were performed, and the obtained results are as follows:

1 [(PC-HCl)(QL)]: $C_{19}H_{27}N_2O_4Cl$; mol. wt. = 382.92; calc.: %C, 59.54; %H, 7.05; %N, 7.31, found: %C, 60.01; %H, 7.38; %N, 7.73.
2 [(PC-HCl)(PA)]; $C_{19}H_{24}N_5O_9Cl$; mol. wt. = 501.91; calc.: %C, 45.43; %H, 4.78; %N, 13.95, found: %C, 45.11; %H, 4.55; %N, 14.23.
3 [(PC-HCl)(TCNQ)]; $C_{25}H_{25}N_6O_2Cl$; mol. wt. = 477; calc.: %C, 62.89; %H, 5.24; %N, 17.61, found: %C, 63.22; %H, 5.37; %N, 17.25.

The resulting values are in good agreement with the calculated values, and the suggested values are in agreement with the molar ratios determined from the photometric titration curves.

### 3.2. Determination of stoichiometry of the resulting CT complexes

The electronic absorption spectra of PC-HCl, π-acceptors (QL, PA, and TCNQ) and the formed CT complexes are shown in Fig. 1. The spectra demonstrate that the formed CT complexes have new strong absorption bands attributed to the CT interactions. These bands are not present in the spectra of the free reactants and are observed at 296, 395 and 299 nm for the PC-HCl/QL, PC-HCl/PA and PC-HCl/TCNQ complexes, respectively. The peak

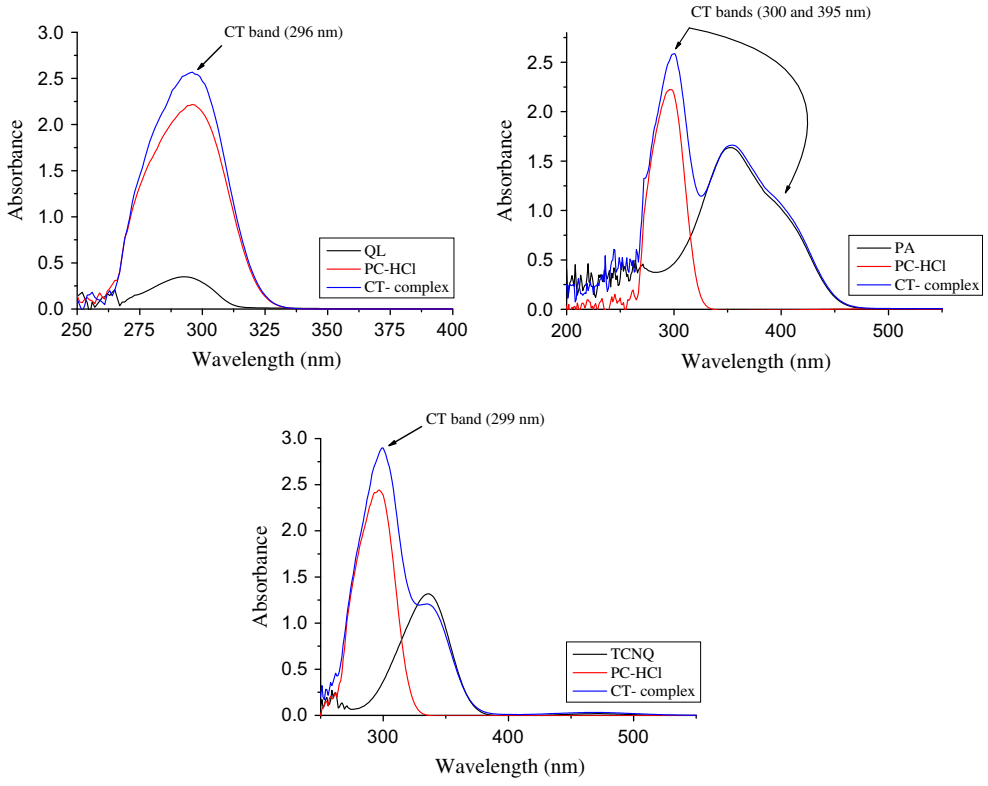


**Fig. 1.** Electronic absorption spectra of PC-HCl CT-complexes at the detectable peak.

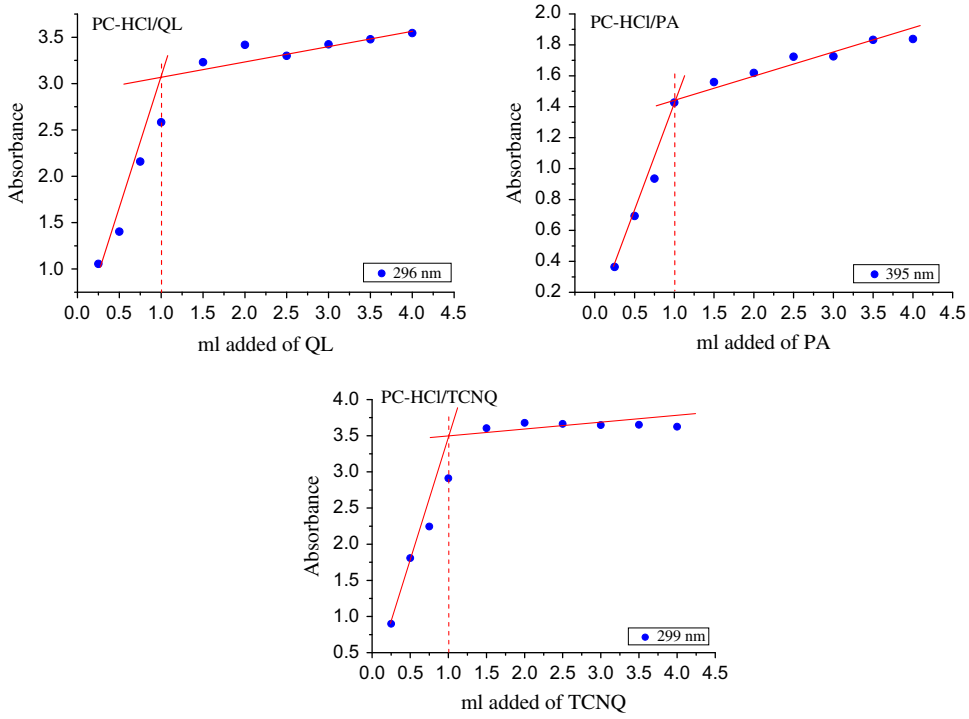


**Fig. 2.** Photometric titration curves for PC-HCl/QL, PC-HCl/PA, and PC-HCl/TCNQ systems at detectable peaks of 296, 395 and 299 nm, respectively.

absorbance values that appeared in the spectra assigned to the formed CT complexes were measured and plotted as function of the $C_d$:$C_a$ ratio according to the known method. Photometric titration plots based on these measurements are shown in Fig. 2. The stoichiometry ratio of the complex formation, PC-HCl: acceptor was found to be 1:1 for all of the complexes. Based on the obtained data, the formed charge transfer complexes were formulated as [(PC-HCl)(QL)], [(PC-HCl)(PA)] and [(PC-HCl)(TCNQ)].

### *3.3. Determination of the formation constant and the molar extinction coefficient*

The spectrophotometric titrations of the intermolecular charge-transfer complexes formed from the reactions of PC-HCl with QL, PA and TCNQ acceptors indicated the formation of 1:1 CT complexes; therefore, the formation constant ($K_{CT}$) and the molar absorptivity ($\varepsilon$) of these complexes were calculated by

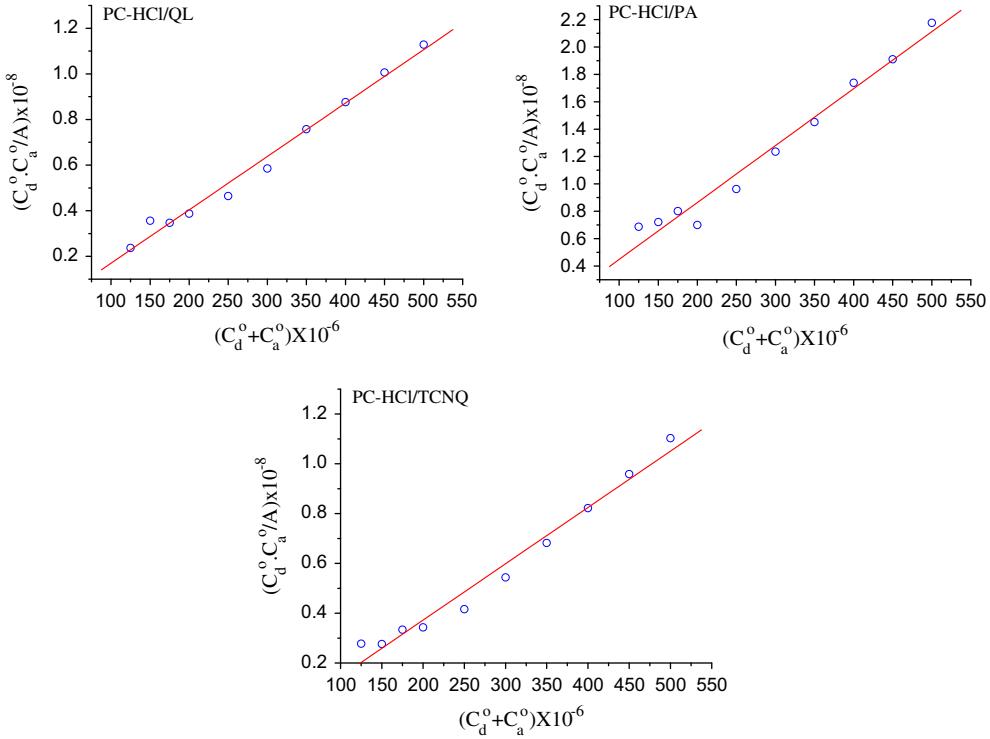


**Fig. 3.** The modified Benesi–Hildebrand plots of PC-HCl/QL, PC-HCl/PA and PC-HCl/TCNQ systems at detectable peaks of 296, 395 and 299 nm, respectively.

**Table 1**
Spectrophotometric results of the PC-HCl CT-complexes.

| Complex | $\lambda_{max}$ (nm) | $E_{CT}$ (eV) | $K$ (L mol$^{-1}$) | $\varepsilon_{max}$ (L mol$^{-1}$ cm$^{-1}$) | $f$ | $\mu$ | $I_P$ | $D$ | $R_N$ | $\Delta G^\circ$ (25 °C) (kJ mol$^{-1}$) |
|---|---|---|---|---|---|---|---|---|---|---|
| PC-HCl/QL | 296 | 4.20 | $3.66 \times 10^4$ | $4.27 \times 10^4$ | 46.14 | 53.87 | 10.93 | 32.70 | 1.19 | −37,446 |
| PC-HCl/PA | 395 | 3.15 | $3.44 \times 10^4$ | $2.40 \times 10^4$ | 10.38 | 29.52 | 9.63 | 32.70 | 0.89 | −40,522 |
| PC-HCl/TCNQ | 299 | 4.16 | $2.81 \times 10^4$ | $4.43 \times 10^4$ | 27.30 | 41.65 | 10.88 | 32.70 | 1. 18 | −36,795 |

applying the 1:1 modified Benesi–Hildebrand equation in Eq. (1) [35]:

$$(C_aC_d)/A = 1/K\varepsilon + (C_a + C_d)/\varepsilon \quad (1)$$

where $C_a$ and $C_d$ are the initial concentrations of the acceptor and the donor, respectively, and $A$ is the absorbance of the strong detected CT band. When the $(C_aC_d)/A$ values for the 1:1 charge transfer complex are plotted against the corresponding $(C_a + C_d)$ values, a straight line is obtained with a slope of $1/\varepsilon$ and an intercept of $1/K\varepsilon$. The modified Benesi–Hildebrand plots are shown in Fig. 3, whereas the obtained $K_{CT}$ and $\varepsilon$ values are shown in Table 1. In general, these complexes exhibit high values for both the formation constants ($K_{CT}$) and the extinction coefficients ($\varepsilon$). The high values of $K_{CT}$ reflect the expected high stabilities of the formed CT complexes as a result of the expected strong donation from the PC-HCl drug that contains two amino groups and one acetate group. The data also reveal that the [(PC-HCl)(QL)] complex exhibits higher values for both $K_{CT}$ and $\varepsilon_{CT}$ compared with the other two complexes.

### 3.4. Determination of the spectroscopic and physical data

The spectroscopic and physical data, such as the standard free energy ($\Delta G^\circ$), the oscillator strength ($f$), the transition dipole moment ($\mu$), the resonance energy ($R_N$), and the ionization potential ($I_P$), were estimated for samples dissolved in methanol at 25 °C. The calculations can be summarized as follow;

From the CT absorption spectra, the oscillator strength ($f$) can be estimated using the approximate formula [43]:

$$f = 4.319 \times 10^{-9} \int \varepsilon_{CT} dv \quad (2)$$

where $\int \varepsilon_{CT}\, dv$ is the area under the curve of the extinction coefficient of the absorption band in question plotted as a function of frequency. To a first approximation,

$$f = 4.319 \times 10^{-9} \varepsilon_{CT} v_{1/2} \quad (3)$$

where $\varepsilon_{CT}$ is the maximum extinction coefficient of the CT band, and $v_{1/2}$ is the half-bandwidth in cm$^{-1}$, i.e., the width of the band at half the maximum extinction. The transition dipole moment ($\mu$) of the PC-HCl CT complexes have been calculated from Eq. (4) [44]:

$$\mu = 0.0958[\varepsilon_{CT} v_{1/2}/v_{max}]^{1/2} \quad (4)$$

The transition dipole moment is useful for determining if the transitions are allowed; the transition from a bonding π orbital to an antibonding π* orbital is allowed because the integral that defines the transition dipole moment is nonzero. The ionization potentials ($I_P$) of the PC-HCl donors in their charge-transfer complexes were calculated using the empirical equation derived by Aloisi and Pignataro represented in Eq. (5) [45]:

$$I_P\ (\text{eV}) = 5.76 + 1.53 \times 10^{-4} v_{CT} \quad (5)$$

where $v_{CT}$ is the wavenumber in cm$^{-1}$ that corresponds to the CT band formed from the interaction between the donor and the acceptor. The electron-donating power of a donor molecule is measured by its ionization potential, which is the energy required to remove an electron from the highest occupied molecular orbital. Briegleb and Czekalla [46] theoretically derived the relationship to obtain the resonance energy ($R_N$), which given below:

$$\varepsilon_C T = 7.7 \times 10^{-4}/[hv_{CT}/[R_N] - 3.5] \quad (6)$$

where $\varepsilon_{CT}$ is the molar absorptivity coefficient of the CT complex at the maximum of the CT absorption, $v_{CT}$ is the frequency of the CT peak, and $R_N$ is the resonance energy of the complex in the ground state, which contributes to the stability constant of the complex (a ground-state property). The energy ($E_{CT}$) of the n → π* and π–π* interactions between the donor (PC-HCl) and the acceptors was calculated using the equation derived by Briegleb [47]:

$$E_{CT} = (hv_{CT}) = (1243.667/\lambda_{CT}) \quad (7)$$

where $\lambda_{CT}$ is the wavelength of the CT band. The standard free energy changes of complexation ($\Delta G^\circ$) were calculated from the formation constants using the equation derived by Martin et al. [48]:

$$\Delta G^\circ = -2.303RT \log K_{CT} \quad (8)$$

where $\Delta G^\circ$ is the free energy change of the CT complexes (kJ mol$^{-1}$), $R$ is the gas constant (8.314 J mol$^{-1}$K), $T$ is the absolute temperature in K, and $K_{CT}$ is the formation constant of the complex (L mol$^{-1}$) at room temperature.

The calculated spectroscopic and physical values ($f$, $\mu$, $I_P$, $R_N$ and $\Delta G^\circ$) for the PC-HCl complexes using these Eqs. (2)–(8) are presented in Table 1. The [(PC-HCl)(QL)] complex exhibits considerably higher values of both oscillator strength ($f$) and transition dipole moment ($\mu$) compared to the other complexes. The observed high values of $f$ indicate a strong interaction between the donor–acceptor pairs with relatively high probabilities of CT transitions [49]. Among the numerous applications of CT complexes, one important application is the calculation of the ionization potential ($I_P$) of the donor. The calculated $I_P$ value for the highest filled molecular orbital that participates in the CT interaction of the PC-HCl drug is approximately 10.45. The ionization potential of the electron donor has been reported to be correlated with the charge-transfer transition energy of the complex [50]. Further evidence for the nature of CT interactions is the calculation of the standard free energy change ($\Delta G^\circ$). The obtained values of $\Delta G^\circ$ for the PC-HCl/QL, PC-HCl/PA and PC-HCl/TCNQ are −37.5, −40.5 and −36.8 kJ mol$^{-1}$, respectively; these values indicate that the interaction between the PC-HCl and the acceptors is exothermic and spontaneous. The $\Delta G^\circ$ values, in general, are more negative as the formation constants of the CT complexes increase. The values of $\Delta G^\circ$ become more negative as the bond between the components becomes stronger and the components are therefore subjected to more physical strain or loss of freedom.

### 3.5. IR and Raman spectra

Infrared and Raman spectral studies shed light on the donation location in the donor species, and the differences occur in the spectra of the obtained charge-transfer complexes. The peak assignments for the important characteristic IR and Raman spectral bands for the formed PC-HCl charge-transfer complexes are shown in Table 2, whereas the full assignments for all of the IR bands in the spectrum are listed in Tables 3–5. The full IR and Raman spectra of the CT complexes are shown in Figs. 4 and 5, respectively. A

**Table 2**
Assignments of the characteristic IR and Raman spectral bands ($cm^{-1}$) for [PC-HCl)(QL)] and [(PC-HCl)(PA)] complexes.

| Complex | $\nu$(NH) | | $\delta(NH_3^+)_{def}$ | | $\delta(NH_3^+)_{sym}$ | | $\rho(NH_3^+)$ | |
|---|---|---|---|---|---|---|---|---|
| | IR | Raman | IR | Raman | IR | Raman | IR | Raman |
| [(PC-HCl)(QL)] | 3201 | 3057 | 1607 | 1606 | 1311 | 1267 | 845 | 867 |
| [(PC-HCl)(PA)] | 3174 | 3008 | 1609 | 1554 | 1338 | 1335 | 801 | 825 |

**Table 3**
Characteristic infrared frequencies ($cm^{-1}$)[a,b] and tentative assignments for PC-HCl, QL and their complex.

| PC-HCl | QL | Complex [(PC-HCl)(QL)] | Assignments[b] |
|---|---|---|---|
| 3361 s | 3262 br | 3384 s | $\nu$(N—H); PC-HCl |
| 3315 s | 3031 m | 3359 sh | $\nu_{as}$(C—H); PC-HCl |
| 3207 s | | 3302 s | $\nu$(O—H); QL |
| | | 3201 ms | $\nu$(C—H); aromatic |
| | | | $\nu(NH_3^+)$ |
| 2955 vs | 2857 m | 2948 ms | $\nu_s$(C—H) + $\nu_{as}$(C—H) |
| 2854 vs | 2836 m | 2880 w | Hydrogen bonding |
| | 2716 m | 2762 w | |
| | | 2665 ms | |
| 2587 s | 2590 w | 2483 mw | $\nu(^+N—H)$; PC-HCl |
| 2496 s | 2467 vw | | |
| 1694 vs | 1866 m | 1686 vs | $\nu$(C=O); PC-HCl |
| | 1855 m | | |
| 1645 ms | 1628 w | 1607 vs | $\delta$(N—H); PC-HCl |
| 1606 vs | 1609 w | 1517 vs | $\delta(NH_3^+)_{def}$, complex |
| 1520 ms | 1518 vs | | $\nu$(C=C) (in-ring), aromatic |
| | | | $\nu$(C=O) + $\nu$(C=N) |
| | | | $\delta$(C—H) deformation |
| | | | Ring breathing bands |
| 1453 vs | 1477 vs | 1466 s | $\nu$(C—H); alkanes; PC-HCl |
| | | | $\nu$(C=C) (in-ring), aromatic |
| | | | $\delta$(C—H) deformation |
| 1363 s | 1366 ms | 1360 mw | $\delta(NH_3^+)_{sym}$, complex |
| | | 1311 s | $\nu$(C—C) + $\nu$(C—O) + $\nu_{as}$(C—N) |
| | | | C—H rock, alkanes; PC-HCl |
| 1316 s | 1244 vs | 1281 vs | $\nu_s$(C—N); PC-HCl |
| 1272 vs | 1222 vs | 1243 m | |
| 1173 s | 1210 vs | 1210 ms | $\nu$(C—O); PC-HCl, QL |
| 1116 s | 1164 ms | 1173 ms | $\delta$(C—H) in plane bending |
| 1074 m | 1097 m | 1116 s | $\delta_{rock}$; NH |
| 1049 m | | 1008 m | |
| 850 s | 827 s | 845 ms | $\rho(NH_3^+)$, complex |
| 771 vs | 759 vs | 763 s | C—H out of plane bending |
| | | | $\delta_{rock}$, $CH_2$ rock |
| | | | N—H wag skeletal vibrations |
| 638 m | 616 m | 624 m | CNC deformation |
| | 525 ms | 515 m | |

[a] s, strong; w, weak; m, medium; sh, shoulder; v, very; vs very strong; br, broad.
[b] $\nu$, stretching; $\nu_s$, symmetrical stretching; $\nu_{as}$, asymmetrical stretching; $\delta$, bending.

**Table 4**
Characteristic infrared frequencies ($cm^{-1}$)[a,b] and tentative assignments for PC-HCl, PA and their complex.

| PC-HCl | PA | Complex [(PC-HCl)(PA)] | Assignments[b] |
|---|---|---|---|
| 3361 s | 3416 br | 3404 m, br | $\nu$(N—H); PC-HCl |
| 3315 s | 3103 ms | 3174 m | $\nu_{as}$(C—H); PC-HCl |
| 3207 s | | 3079 m | $\nu$(O—H); PA |
| | | 3003 m | $\nu$(C—H); aromatic |
| | | | $\nu(NH_3^+)$ |
| 2955 vs | 2980 sh | 2798 m | $\nu_s$(C—H) + $\nu_{as}$(C—H) |
| 2854 vs | 2872 w | 2742 m, br | Hydrogen bonding |
| 2587 s | – | – | $\nu(^+N—H)$; PC-HCl |
| 2496 s | | | |
| 1694 vs | – | 1737 vs | $\nu$(C=O); PC-HCl |
| 1645 ms | 1632 vs | 1609 vs | $\delta$(N—H); PC-HCl |
| 1606 vs | 1608 vs | 1560 vs | $\nu_{as}(NO_2)$; PA |
| 1520 ms | 1529 vs | | $\delta(NH_3^+)_{def}$, complex |
| | | | $\nu$(C=C) (in-ring), aromatic |
| | | | $\nu$(C=O) + $\nu$(C=N) |
| | | | $\delta$(C—H) deformation |
| | | | Ring breathing bands |
| 1453 vs | 1432 s | 1428 ms | $\nu$(C—H); alkanes; PC-HCl |
| | | | $\nu$(C=C) (in-ring), aromatic |
| | | | $\delta$(C—H) deformation |
| 1363 s | 1343 ms | 1338 vs | $\delta(NH_3^+)_{sym}$, complex |
| | 1312 w | | $\nu$(C—C) + $\nu$(C—O) + $\nu_{as}$(C—N) |
| | | | C—H rock, alkanes; PC-HCl |
| | | | $\nu_s NO_2$ |
| 1316 s | 1263 w | 1271 vs | $\nu_s$(C—N); PC-HCl |
| 1272 vs | 1150 ms | 1165 ms | $\nu$(C—O); PC-HCl, PA |
| 1173 s | 1086 s | 1110 s | $\delta$(C—H) in plane bending |
| 1116 s | 917 vs | 1080 m | $\delta_{rock}$; NH |
| 1074 m | | 1014 m | |
| 1049 m | | 915 m | |
| 850 s | 829 w | 801 m | $\rho(NH_3^+)$, complex |
| 771 vs | 781 s | 751 m | C—H out of plane bending |
| | 732 s | 714 s | $\delta_{rock}$, $CH_2$ rock |
| | | | N—H wag skeletal vibrations |
| 638 m | 703 s | 634 mw | $\delta$(ONO); PA |
| | 652 sh | 542 mw | CNC deformation |
| | 522 ms | | |

[a] s, strong; w, weak; m, medium; sh, shoulder; v, very; vs very strong; br, broad.
[b] $\nu$, stretching; $\nu_s$, symmetrical stretching; $\nu_{as}$, asymmetrical stretching; $\delta$, bending.

comparison of the relevant IR spectral bands of the free donor, PC-HCl and acceptors (QL, PA, and TCNQ) with the corresponding bands in the IR spectra of the isolated solid CT complexes clearly indicated that the characteristic bands of PC-HCl exhibit small shifts in frequency (Tables 3–5) and changes in their band intensities. This result could be attributed to the expected changes in symmetry and electronic configurations upon the formation of the CT complexes. The IR spectra of the PC-HCl/QL and PC-HCl/PA complexes are characterized by a broad medium band that appears between 2400 and 2800 $cm^{-1}$ (2665 $cm^{-1}$ for the QL complex; 2742 $cm^{-1}$ for the PA complex), which does not appear in the spectra of the free PC-HCl donor or those of the QL and PA acceptors. These bands are attributed to the stretching vibration of the intermolecular hydrogen bond formed through the transfer of proton from the acidic center on the QL and PA acceptors to the basic center of the PC-HCl donor (—$NH_2$) [51]. This assumption is strongly supported by the appearance of the main characteristic absorption bands that result from the stretching and bending deformation of the $NH_3^+$ group. For example, the *$\nu$(NH)*, $\nu_{def}(NH_3^+)$, $\delta_{sym}(NH_3^+)$ and $\rho(NH_3^+)$ vibrations in the [(PC-HCl)(QL)] and [(PC-HCl)(PA)] complexes occur at approximately 3200, 1600, 1300 and 800 $cm^{-1}$, respectively. The presence of these bands confirmed that the complexation occurs through the protonation of the —$NH_2$ group of the PC-HCl donor via a proton-transfer phenomenon from the acidic center of each acceptor to the lone pair of electrons on

**Table 5**
Characteristic infrared frequencies ($cm^{-1}$)[a,b] and tentative assignments for PC-HCl, TCNQ and their complex.

| PC-HCl | TCNQ | Complex [(PC-HCl)(TCNQ)] | Assignments[b] |
|---|---|---|---|
| 3361 s<br>3315 s<br>3207 s | 3137 ms<br>3050 s | 3740 vw<br>3618 vw<br>3135 m, br<br>3049 m | $\nu$(N—H); PC-HCl<br>$\nu_{as}$(C—H); PC-HCl<br>$\nu$(C—H); aromatic |
| 2955 vs<br>2854 vs | 2969 mw<br>2851 mw | – | $\nu_s$(C—H) + $\nu_{as}$(C—H) |
| 2587 s<br>2496 s | 2220 s | 2690 w, br<br>2179 vs<br>2135 s | $\nu$($^+$N—H); PC-HCl<br><br>$\nu$(C≡N); TCNQ |
| 1694 vs | – | 1718 s | $\nu$(C=O); PC-HCl |
| 1645 ms<br>1606 vs<br>1520 ms | 1540 vs | 1597 w<br>1563 vs | $\delta$(N—H); PC-HCl<br>$\nu$(C=C) (in-ring), aromatic<br>$\nu$(C=O) + $\nu$(C=N)<br>$\delta$(C—H) deformation<br>Ring breathing bands |
| 1453 vs | – | 1433 vw<br>1404 m | $\nu$(C—H); alkanes; PC-HCl<br>$\nu$(C=C) (in-ring), aromatic<br>$\delta$(C—H) deformation |
| 1363 s | 1352 ms | 1333 s | $\nu$(C—C) + $\nu$(C—O) + $\nu_{as}$(C—N)<br>C—H rock, alkanes; PC-HCl |
| 1316 s<br>1272 vs<br>1173 s<br>1116 s<br>1074 m<br>1049 m | 1285 vw<br>1205 vw<br>1117 ms<br>1044 vw | 1270 vs<br>1179 s<br>1109 ms<br>1017 m | $\nu_s$(C—N); PC-HCl<br>$\nu$(C—O); PC-HCl, QL<br>$\delta$(C—H) in plane bending<br>$\delta_{rock}$; NH |
| 850 s<br>771 vs | 997 vw<br>962 vw<br>860 vs<br>808 vw | 861 m<br>770 m | C—H out of plane bending<br>$\delta_{rock}$, $CH_2$ rock<br>N—H wag skeletal vibrations |
| 638 m | 473 vs | 631 vw<br>573 vw<br>476 w | CNC deformation |

[a] s, strong; w, weak; m, medium; sh, shoulder; v, very; vs very strong; br, broad.
[b] stretching; $\nu_s$, symmetrical stretching; $\nu_{as}$, asymmetrical stretching; $\delta$, bending.

the —$NH_2$ group in the PC-HCl donor to form $NH_3^+$ ammonium based on acid–base theory [52–54].

In the IR spectra of the [(PC-HCl)(TCNQ)] complex, the characteristic bands of PC-HCl ($\nu$(—$NH_2$); 3361 and 3315 $cm^{-1}$) exhibit a significant decrease in intensity, and the band that results from the $\nu$(C≡N) vibration of the free TCNQ acceptor that appeared at 2220 $cm^{-1}$ shifted to 2135 $cm^{-1}$ in the complex. This observation clearly indicates that the —$NH_2$ group in the donor and the —C≡N group in the acceptor participated in the complexation process. Because TCNQ lacks acidic centers, the molecular complexes can be concluded to form through $\pi \rightarrow \pi^*$ and/or $n \rightarrow \pi^*$ charge migration from the HOMO of the donor to the LUMO of the acceptor. The $\pi \rightarrow \pi^*$ CT complex is formed via the benzene ring (electron-rich group) of the PC-HCl drug and the TCNQ reagent (electron acceptor) [55,56]. However, the absence of a few bands at approximately 2600–2400 $cm^{-1}$ (hydrogen bonding) in the spectrum of this complex strongly indicates that the interaction mode between PC-HCl and the TCNQ acceptor occurs through the migration of a $H^+$ ion to one of the cyano groups in the acceptors to form a positive ion (—C≡N$^+$H) that associates with the anion to form ion pairs [57,58]. The cyano group (—C≡N) is an electron-withdrawing group that exists in TCNQ in a conjugated bonding system. The 4CN groups in TCNQ withdraw electrons from the aromatic ring, and such a process will make the aromatic ring an electron-accepting region. The $\pi^*$–CN electron density appears to increase and more easily accept a proton from the donor because of the electron-withdrawing process and the conjugated electron system. This behavior will decrease the CN bond order and therefore lower its vibrational wavenumber value upon complexation.

### 3.6. $^1$H NMR spectra

The $^1$H NMR spectra of PC-HCl complexes were measured in DMSO-$d_6$, $\delta$ ppm, 400 MHz at room temperature and are given in Fig. 6. The chemical shifts ($\delta$) of the different types of protons of the CT complexes are given below. The results obtained from elemental analyses, infrared spectra, and photometric titrations are in agreement with the $^1$H NMR spectra, which allows an interpretation of the mode of interaction between the donor and the acceptor. The reaction of PC-HCl as the donor with QL as the acceptor yielded a new charge-transfer complex, 4-((2-(diethylammonio)ethoxy)carbonyl)benzenaminium 4-hydroxyphenolate chloride, which produced signals at (Fig. 6): $\delta$ = 1.22 (t, 6H, $2CH_3$), 3.15 (2q, 4H, $2CH_2$), 3.45 (t, 2H, N$^+$—$CH_2$), 4.51 (t, 2H, O—$CH_2$), 6.10 (b, 3H, $NH_3^+$ hydrogen bonded with picrate), 6.58 (2d appear t, 4H, Ar—H phenolate protons), 6.68–7.70 (2d, 4H, Ar—H, anilinium protons), 8.71 (s, 1H, Ar—O<u>H</u>, phenolate), and 10.74 (b, 1H, $NH^+Cl^-$). The $^1$H NMR spectrum of this complex indicated that the phenolic proton (—OH) signal, which is observed at $\delta \sim 8.59$ ppm in the spectrum of the QL acceptor, decreased in intensity with a downfield shift for the non-hydrogen-bonded one ($\delta \sim 8.71$) in the spectrum of the CT complex. This result indicates the involvement of one —OH group in chelating through the deprotonation from the QL acceptor to the PC-HCl donor and an overall decrease of the negative charge on the quinol ring due to the formation of the complex. In addition, the disappearance of the —$NH_2$ protons (PC-HCl) and the appearance of a signal at 6.10 ppm indicate the involvement of the —$NH_2$ groups in the complexation process. The $^1$H NMR spectrum also presents a signal at $\delta$ = 10.74, which is assigned to the $NH^+Cl^-$ proton. Based on these data, the structure suggested for the PC-HCl/QL complex is shown in Formula II.

The reaction between PC-HCl and PA afforded 4-((2-(diethylammonio)ethoxy)carbonyl)benzenaminium 2,4,6-trinitrophenolate chloride. $^1$H NMR (DMSO-$d_6$, $\delta$ ppm) (Fig. 6): $\delta$ = 1.24 (t, 6H, $2CH_3$), 3.20 (2q, 4H, $2CH_2$), 3.66 (t, 2H, N$^+$—$CH_2$), 4.49 (t, 2H, O—$CH_2$), 4.50 (b, 3H, $NH_3^+$ hydrogen bonded with picrate), 6.69 (d, 2H, Ar—H, at C(2 and 6) anilinium ring), 7.73 (d, 2H, Ar—H, at C(3 and 5) anilinium ring), 8.79 (s, 2H, Ar—H, picrate protons), 9.82 (b, 1H, $NH^+Cl^-$). The $^1$H NMR spectrum of this complex revealed that the signal at $\delta$ = 11.94 ppm, which is assigned to the —OH proton of the free picric acid acceptor [55], was absent in the spectrum of this complex, which is attributed to the formation of the CT complex. The formation of the complex was confirmed by the appearance of the characteristic broad signal observed at 4.50 ppm in the spectrum of the complex; this signal is attributed to the formation of ($NH_3^+$) with the disappearance of the (—$NH_2$) signal. The $^1$H NMR confirms that the reaction between PC-HCl and PA occurred in a 1:1 ratio, and the suggested structure of this complex is given in Formula III.

The $^1$H NMR spectrum for the CT complex between PC-HCl and TCNQ is shown in Fig. 6 and is summarized as follows: $\delta$ = 1.28 (t, 6H, $2CH_3$), 3.16 (2q, 4H, $2CH_2$), 3.67 (t, 2H, N$^+$—$CH_2$), 4.57 (t, 2H, O—$CH_2$), 6.41 (s, H, $NH^+$ hydrogen bonded with TCNQ), 6.60 (d, 2H, Ar—H Ar—H, anilinium protons), 7.04 (2d, 4H, Ar—H, anilinium protons), 7.23 (d, 2H, Ar—<u>H</u>, TCNQ C2,C6), 7.33 (d, 2H, Ar—<u>H</u>, TCNQ C3, C5), 7.50 (s, H, Ar—<u>H</u>, $NH^-$), 10.14 (b, 1H, $NH^+Cl^-$). In the charge-transfer reaction between PC-HCl and TCNQ, the proton of the —$NH_2$ group in PC-HCl is transferred to a nitrogen atom of TCNQ to form an ion-paired compound, specifically 4-((2-(diethylammonio)ethoxy)carbonyl)benzenamidocyano [4-(dicyanomethylene)cyclohexa-2,5-dien-1-ylidene]ethanenitrilium chloride. Two

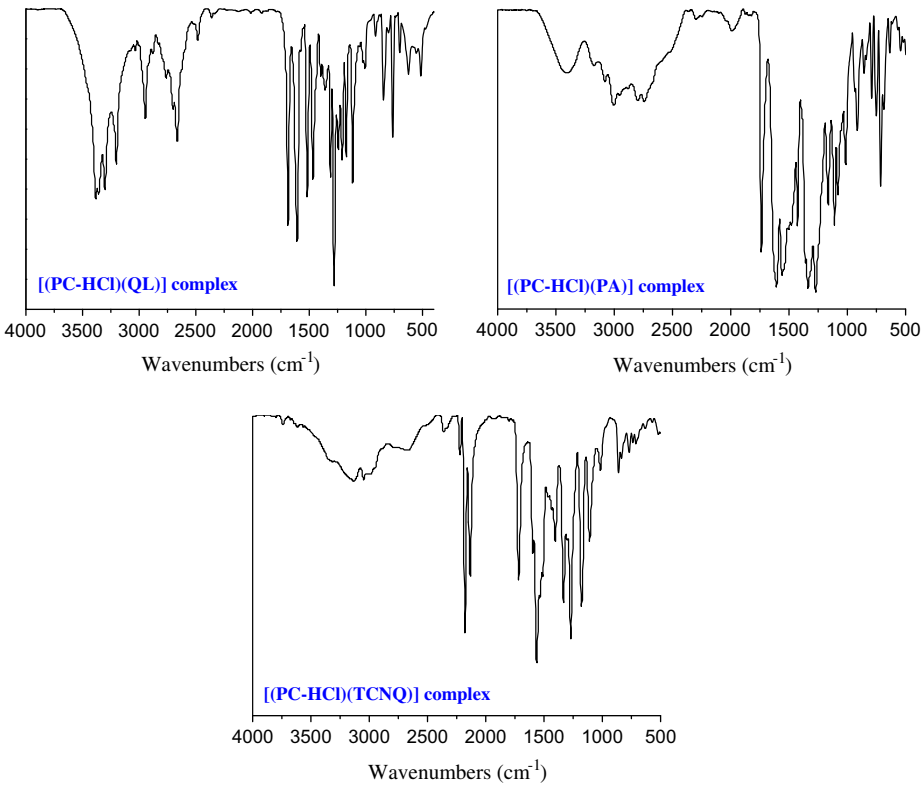


**Fig. 4.** Infrared spectra of PC-HCl CT-complexes.

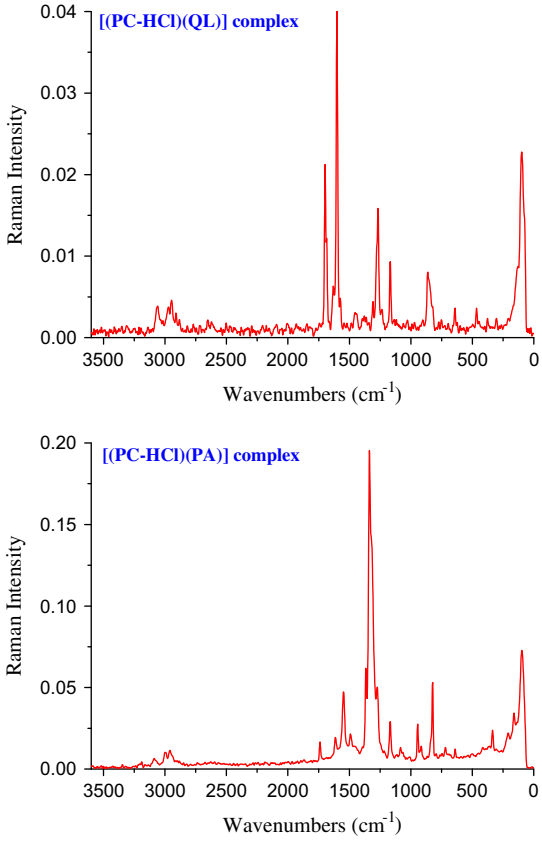


**Fig. 5.** Raman spectra of PC-HCl CT-complexes.

new signals were observed in the $^1$H NMR spectrum of this CT complex at 6.41 and 7.50 ppm, which are assigned to the protons of ($NH^+$) and ($NH^-$), respectively. These signals are not detected in the spectrum of the free donor, which indicates that the —$NH_2$ and —C≡N groups are primarily involved in the formation of the CT complex between PC-HCl and TCNQ. The migration of the $H^+$ ion from the $NH_2$ in the donor to one of the four cyano groups in the TCNQ acceptor resulted in the formation of a positive ion (—C≡$N^+$H), which is associated with the anion $NH^-$; this result is also confirmed from the disappearance of the —$NH_2$ signal in the spectrum of PC-HCl. Because of the formation of the CT complex between PC-HCl and TCNQ, the four similar protons on the aromatic ring of TCNQ became two doublet signals that appeared at $\delta$ 7.23 ($C_2$, C6) and 7.33 ($C_3$, $C_5$) ppm. The intensities and chemical shifts of the aromatic signals were significantly affected by the complexation process and the accompanying changes in the structural configuration. According to these observations, the suggested structure of PC-HCl/TCNQ complex is illustrated in Formula I.

### 3.7. Thermogravimetric studies

The thermogravimetric analysis provided information about the thermal stabilities of the prepared charge-transfer complexes and about the differences in the physical behavior of the starting and resulting compounds [59]. The PC-HCl CT complexes are stable at room temperature and can be stored for several months without any changes. The obtained complexes were studied by thermogravimetric analysis from ambient temperature to 800 °C under air atmosphere. The TG curves were redrawn as mg mass loss versus temperature (TG). Typical TG curves of PC-HCl CT complexes are presented in Fig. 7, and the thermoanalytical results are listed in Table 6. Based on the TG curves, the overall loss of mass is 100% for [(PC-HCl)(QL)], 99.99% for [(PC-HCl)(PA)] and 82.65% for [(PC-HCl)(TCNQ)].

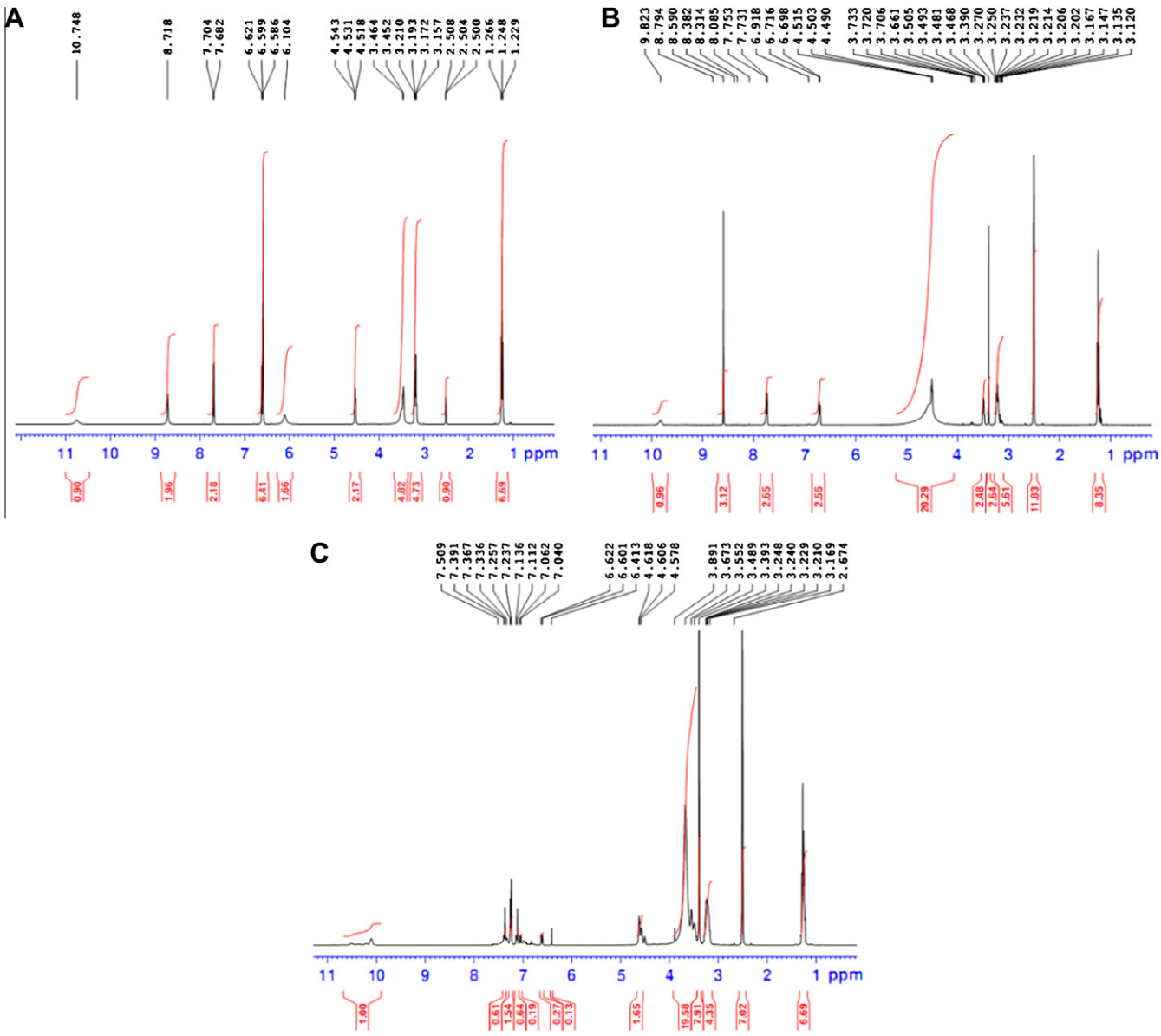


**Fig. 6.** $^{1}H$ NMR spectrum of (A) PC-HCl/QL, (B) PC-HCl/PA and (C) PC-HCl/TCNQ complexes.

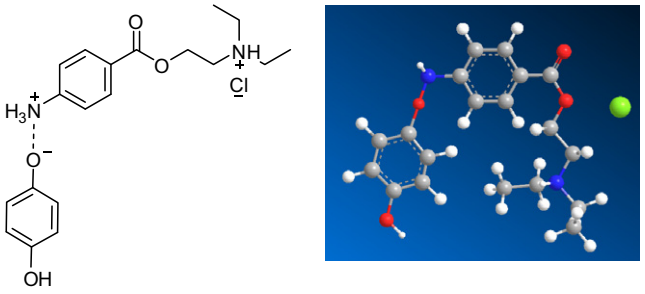


**Formula II.** Suggested structure of the [(PC-HCl)(QL)] complex.

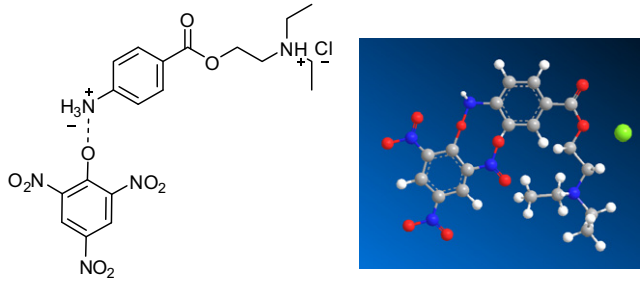


**Formula III.** Suggested structure of the [(PC-HCl)(PA)] complex.

The obtained data indicate that the [(PC-HCl)(QL)] complex is thermally stable in the 25–200 °C temperature range. Decomposition of the complex began at ~200 °C and finished at ~450 °C. The thermal decomposition of the complex is a one-step process within the range of 200–800 °C, which is attributed to the loss of $7C_2H_2$, HCl, $5CO_2$, $NH_3$, $NO_2$ and $4.5H_2$ molecules, representing a weight loss of obs. = 100, cal. = 99.89%. The [(PC-HCl)(PA)] complex began decomposing at ~110 °C in three clear decomposition steps within the 25–800 °C temperature range. The first decomposition step (obs. = 10.19%, calc. = 10.66%) within the temperature range

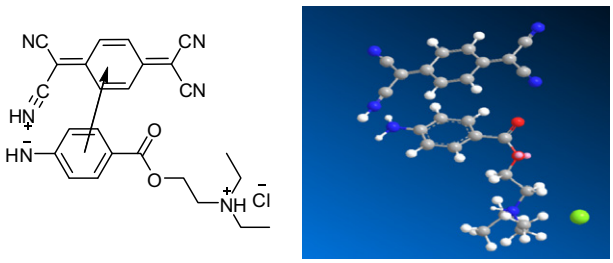

**Formula IV.** Suggested structure for the [(PC-HCl)(TCNQ)] complex.

25–190 °C is attributed to the liberation of HCl and $NH_3$ molecules. The second decomposition step within the 190–315 °C temperature range (obs. = 52.29%, calc. = 51.80%) is reasonably explained by the loss of $3C_2H_2$, $CO_2$ and $3NO_2$ molecules. The third decomposition step existed within the temperature range 315–800, which is reasonably by the loss of $6C_2H_2$, $NO_2$ and $H_2$ molecules. The thermal analysis curve of the [(PC-HCl)(TCNQ)] complex indicates that the decomposition occurs in two main stages in the temperature range of 25–800 °C. The first decomposition step within the temperature range 25–350 °C corresponding to loss of HCl, $2CO_2$, 4HCN and $NH_3$ molecules representing a weight loss of (obs. = 38.11%, calc. = 38.89%). The second decomposition step found within the temperature range 350–800 °C which corresponds to the liberation of $6C_2H_2$, $NO_2$ and $2.5H_2$ molecules with some carbon atoms remaining in the final residue.

### 3.8. Kinetic thermodynamic studies

Thermodynamic parameters: the Coats–Redfern method [60] and the Horowitz–Metzger [61] method.

#### 3.8.1. Coats–Redfern equation

The Coats–Redfern equation (9), which is an atypical integral method, can be represented as:

$$\int_{0\to\infty} d\alpha/(1-\alpha)^n = (A/\varphi)\int_{T1\to T2} e^{-E^*/RT}dT \tag{9}$$

For convenience of integration, the lower limit $T_1$ is usually taken as zero. After integration, this equation can be represented as:

$$\ln[-\ln(1-\alpha)/T^2] = -E^*/RT + \ln[AR/\varphi E^*] \tag{10}$$

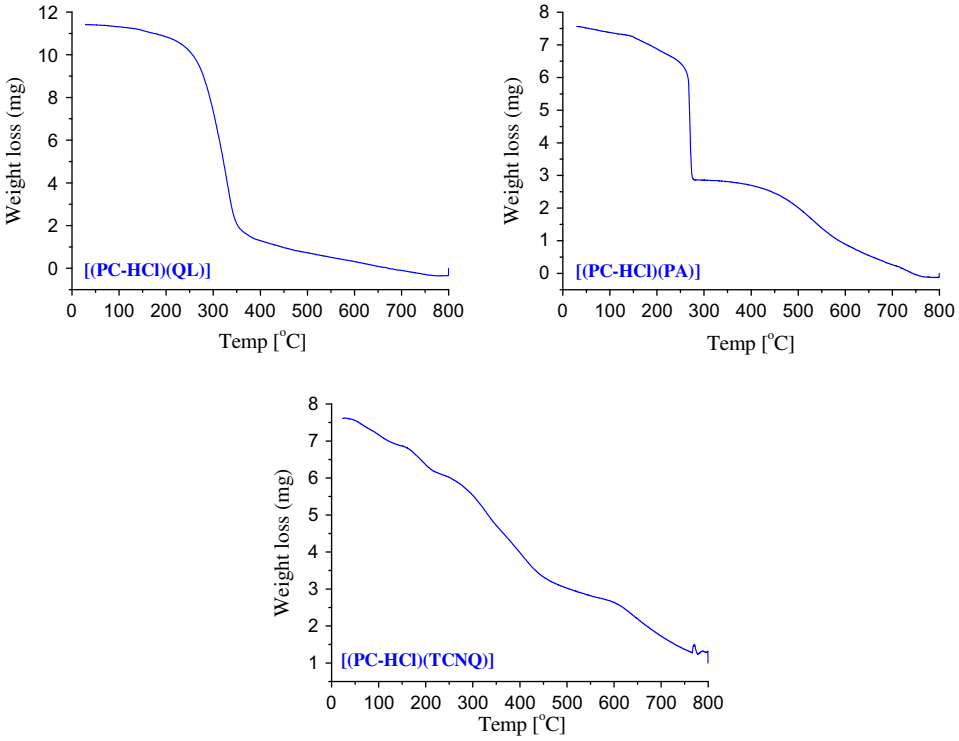


**Fig. 7.** TG curves of PC-HCl CT-complexes.

**Table 6**
Thermal decomposition data for the PC-HCl CT-complexes.

| Complex | Stage | TG range (°C) | Mass loss (%) | | Evolved moiety |
|---|---|---|---|---|---|
| | | | Found | Calculated | |
| PC-HCl/QL ($C_{19}H_{27}N_2O_4Cl$) | I | 25–800 | 100.00 | 99.89 | $7C_2H_2 + HCl + 5CO_2 + NH_3 + NO_2 + 4.5H_2$ |
| PC-HCl/PA ($C_{19}H_{24}N_5O_9Cl$) | I | 25–190 | 10.19 | 10.66 | $HCl + NH_3$ |
| | II | 190–315 | 52.29 | 51.80 | $3C_2H_2 + CO_2 + 3NO_2$ |
| | III | 315–800 | 37.51 | 37.46 | $6C_2H_2 + NO_2 + H_2$ |
| PC-HCl/TCNQ ($C_{25}H_{25}N_6O_2Cl$) | I | 25–350 | 38.11 | 38.89 | $HCl + 2CO_2 + 4HCN + NH_3$ |
| | II | 350–800 | 44.54 | 43.40 | $6C_2H_2 + NO_2 + 2.5H_2$ |
| | Residue | – | 17.35 | 17.61 | 7C |

where $\alpha$ is the fraction of the sample decomposed at time $t$, $T$ is the derivative peak temperature, $A$ is the frequency factor, $R$ is the gas constant, $E^*$ is the activation energy, and $\varphi$ is the linear heating rate. A plot of the left-hand side (LHS) against $1/T$ was constructed. $E^*$ is the energy of activation in kJ mol$^{-1}$ and was calculated from the slope, and $A$ in (s$^{-1}$) was calculated from the intercept. The entropy of activation, $\Delta S^*$, in (J K$^{-1}$ mol$^{-1}$) was calculated using the equation:

$$\Delta S^* = R\ln(Ah/kT_s) \tag{11}$$

where $k$ is the Boltzmann constant, $h$ is Planck's constant, and $T_s$ is the DTG peak temperature.

### 3.8.2. Horowitz–Metzger equation

The Horowitz–Metzger equation (Eq. (12)) was written in the following form:

$$\text{Log}\ [\log\ (w_\alpha/w_\gamma)] = E^*\theta/2.303RT_s^2 - \log 2.303 \tag{12}$$

where $\theta = T - T_s$, $w_\gamma = w_\alpha - w$, $w_\alpha$ is the mass loss at the completion of the reaction, and $w$ is the mass loss at time $t$.

The plot of $\log[\log(w_\alpha/w_\gamma)]$ versus $\theta$ was constructed and was observed to be linear, and the slope, $E^*$, was calculated. The pre-exponential factor, $A$, was calculated from:

$$E^*\theta/RT_s^2 = A/[\varphi\exp(-E^*/RT_s)] \tag{13}$$

From the TG curves, the activation energy, $E^*$, the entropy of activation, $\Delta S^*$, the enthalpy of activation, $\Delta H^*$, and the Gibbs free energy, $\Delta G^*$, were calculated from:

$$\Delta H^* = E^* - RT \quad \text{and} \quad \Delta G^* = \Delta H^* - T\Delta S^*$$

The linear curves from the Coats–Redfern and Horowitz–Metzger plots are shown in Fig. 8, and the evaluated kinetic parameters for the first stages based on the Coats–Redfern and Horowitz–Metzger equations are listed in Table 7. The results indicate that the kinetic data obtained from the two methods are comparable and in agreement with each other. Based on the results in Table 7, the following conclusions are drawn:

1. A higher value of activation energy suggests a higher thermal stability. The [(PC-HCl)(TCNQ)] complex exhibits a higher activation energy value, which indicates the higher thermal stability of this complex.

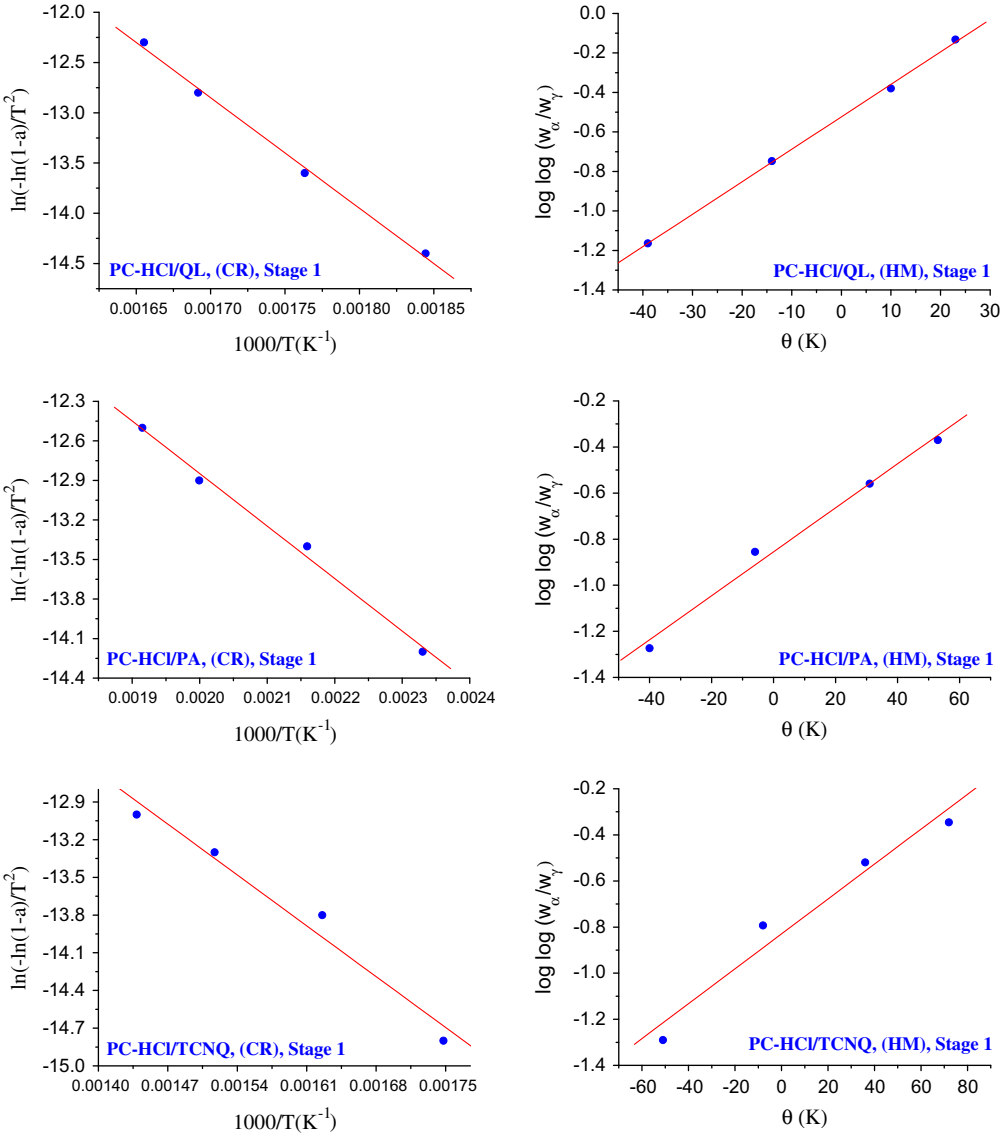


**Fig. 8.** The diagrams of kinetic parameters of PC-HCl complexes using Coats–Redfern (CR) and Horowitz–Metzger (HM) equations.

**Table 7**
Kinetic parameters determined using the Coats–Redfern (CR) and Horowitz–Metzger (HM).

| Complexes | Stage | Method | Parameters[a] | | | | | $r$ |
|---|---|---|---|---|---|---|---|---|
| | | | $E^*$ | $A$ | $\Delta S^*$ | $\Delta H^*$ | $\Delta G^*$ | |
| [(PC-HCl)(QL)] | 1st | CR | $3.31 \times 10^4$ | 7.56 | $-2.32 \times 10^2$ | $2.92 \times 10^4$ | $1.38 \times 10^5$ | 0.99654 |
| | | HM | $4.02 \times 10^4$ | $1.65 \times 10^2$ | $-2.06 \times 10^2$ | $3.63 \times 10^4$ | $1.33 \times 10^5$ | 0.99457 |
| [(PC-HCl)(PA)] | 1st | CR | $3.32 \times 10^4$ | 7.57 | $-2.34 \times 10^2$ | $2.79 \times 10^4$ | $1.74 \times 10^5$ | 0.99654 |
| | | HM | $7.09 \times 10^4$ | $4.85 \times 10^3$ | $-1.80 \times 10^2$ | $6.58 \times 10^4$ | $1.78 \times 10^5$ | 0.99457 |
| [(PC-HCl)(TCNQ)] | 1st | CR | $4.80 \times 10^4$ | $1.48 \times 10^1$ | $-2.29 \times 10^2$ | $4.29 \times 10^4$ | $1.85 \times 10^5$ | 0.98426 |
| | | HM | $5.63 \times 10^4$ | $2.28 \times 10^2$ | $-2.06 \times 10^2$ | $5.11 \times 10^4$ | $1.79 \times 10^5$ | 0.98012 |

[a] Units of parameters: $E$ in kJ mol$^{-1}$, $A$ in s$^{-1}$, $\Delta S$ in J mol$^{-1}$ K$^{-1}$, $\Delta H$ and $\Delta G$ in kJ mol$^{-1}$.

2. The activation energy values ($E^*$) of the PC-HCl complexes arranged in order of thermal stability are [(PC-HCl)(TCNQ)] > [(PC-HCl)(PA)] > [(PC-HCl)(QL)].
3. Satisfactory values for the correlation coefficients from the Arrhenius plots of the thermal decomposition steps were observed to be $r \sim 1$ in all cases, which indicates a good fit with the linear function and reasonable agreement between the experimental data and the kinetic parameters.
4. The thermal decomposition process of all of the PC-HCl complexes is non-spontaneous, i.e., the complexes are thermally stable.

### 3.9. X-ray powder diffraction investigation

To investigate the crystal structures of the obtained PC-HCl CT-complexes, X-ray powder diffraction patterns in the range of $5° < 2\theta < 65°$ for the [(PC-HCl)(QL)] and [(PC-HCl)(PA)] complexes were examined, and the recorded patterns are shown in Fig. 9. An inspection of these patterns reveals that all of the systems are semi-crystalline. As evident from Fig. 9, the main characteristic scattering peak of the [(PC-HCl)(QL)] complex occurs at 17.286°, whereas this peak occurs at 26.723° in the diffraction pattern of the [(PC-HCl)(PA)] complex. Based on these investigations, the sharp and well-defined Bragg peaks at specific $2\theta$ angles confirm the semi-crystalline nature of the investigated CT complexes. The particle size of these two complexes were estimated from their XRD patterns based on the highest intensity value compared with the other peaks using the well-known Debye–Scherrer formula given in Eq. (14) [62]:

$$D = K\lambda/\beta \mathrm{Cos}\theta \quad (14)$$

where $D$ is the apparent particle size of the grains, $K$ is a constant (0.94 for Cu grid), $\lambda$ is the X-ray wavelength used (1.5406 Å), $\theta$ is half the scattering angle (the Bragg diffraction angle), and $\beta$ is the full-width at half-maximum (FWHM) of the X-ray diffraction line (additional peak broadening) in radians.

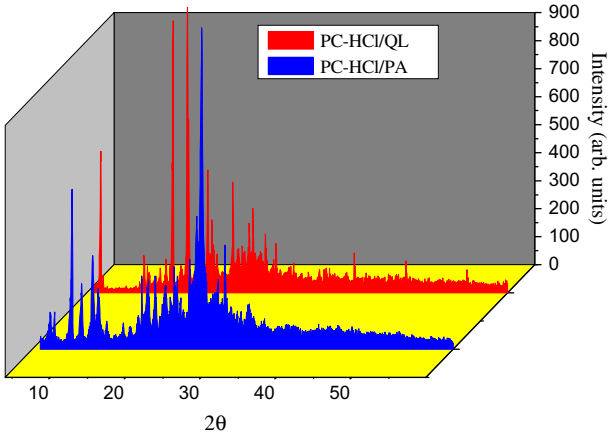


**Fig. 9.** X-ray diffraction pattern for [(PC-HCl)(QL)] and [(PC-HCl)(PA)] complexes.

**Table 8**
XRD spectral data of [(PC-HCl)(QL)] and [(PC-HCl)(PA)] complexes.

| Complex | $2\theta$ (°) | $d$ Value (Å) | Full width at half maximum (FWHM) | Relative intensity (%) | Particle size (nm) |
|---|---|---|---|---|---|
| [(PC-HCl)(QL)] | 17.286 | 5.126 | 0.30 | 100 | 4.880 |
| [(PC-HCl)(PA)] | 26.273 | 3.386 | 0.45 | 100 | 3.306 |

Table 8 presents the XRD spectral data for the [(PC-HCl)(QL)] and [(PC-HCl)(PA)] complexes, including the values of the Bragg angle ($2\theta$), the full-width at half-maximum ($\beta$, FWHM) of the prominent intensity peak, the interplanar spacing between atoms ($d$), the relative intensity and the calculated particle size ($D$) in nm. The particle size of the complexes were estimated according to the highest value of intensity compared with the other peaks and were found to be ~5 and ~3 nm for the [(PC-HCl)(QL)] and [(PC-HCl)(PA)] complexes, respectively. These values confirmed that the particle sizes are located within the nanoscale range.

### 3.10. SEM and EDX studies

Scanning electron microscopy (SEM) provides general information about the microstructure, the surface morphology, the particle size, the microscopic aspects of the physical behavior and the chemical composition of the respective PC-HCl charge-transfer complexes and demonstrates the porous structures of the surface of these complexes. In addition, the chemical compositions of the complexes were determined using energy-dispersive X-ray diffraction (EDX). SEM surface images of the [(PC-HCl)(QL)], [(PC-HCl)(PA)] and [(PC-HCl)(TCNQ)] complexes along with their EDX spectra are shown in Fig. 10. Analysis of the SEM images of the PC-HCl complexes shows that the sizes of the particles are quite different with different acceptors. Furthermore, these images show a small particle size with nanoscale features that have a tendency to form agglomerates with shapes that differ from those of the starting materials. The uniformity and similarity between the particles of the synthesized PC-HCl complexes indicate that the morphological phases of these complexes have a homogeneous matrix. Based on these observations, the [(PC-HCl)(QL)] and [(PC-HCl)(PA)] complexes are semi-crystalline, and some single-phase formations exhibit well-defined shapes with a particle size of ~10 μm. The results also indicate for the particles of the QL complex are flake-shaped and that those of the PA complex are stone-shaped, whereas the [(PC-HCl)(TCNQ)] complex particles exhibits different shapes with a particle size of ~100 μm and a cracked surface. The chemical analysis results from the EDX analysis for the formed complexes show a homogenous distribution of each acceptor. In the EDX profile, the peaks refer to all elements that constitute the molecules of these complexes; these

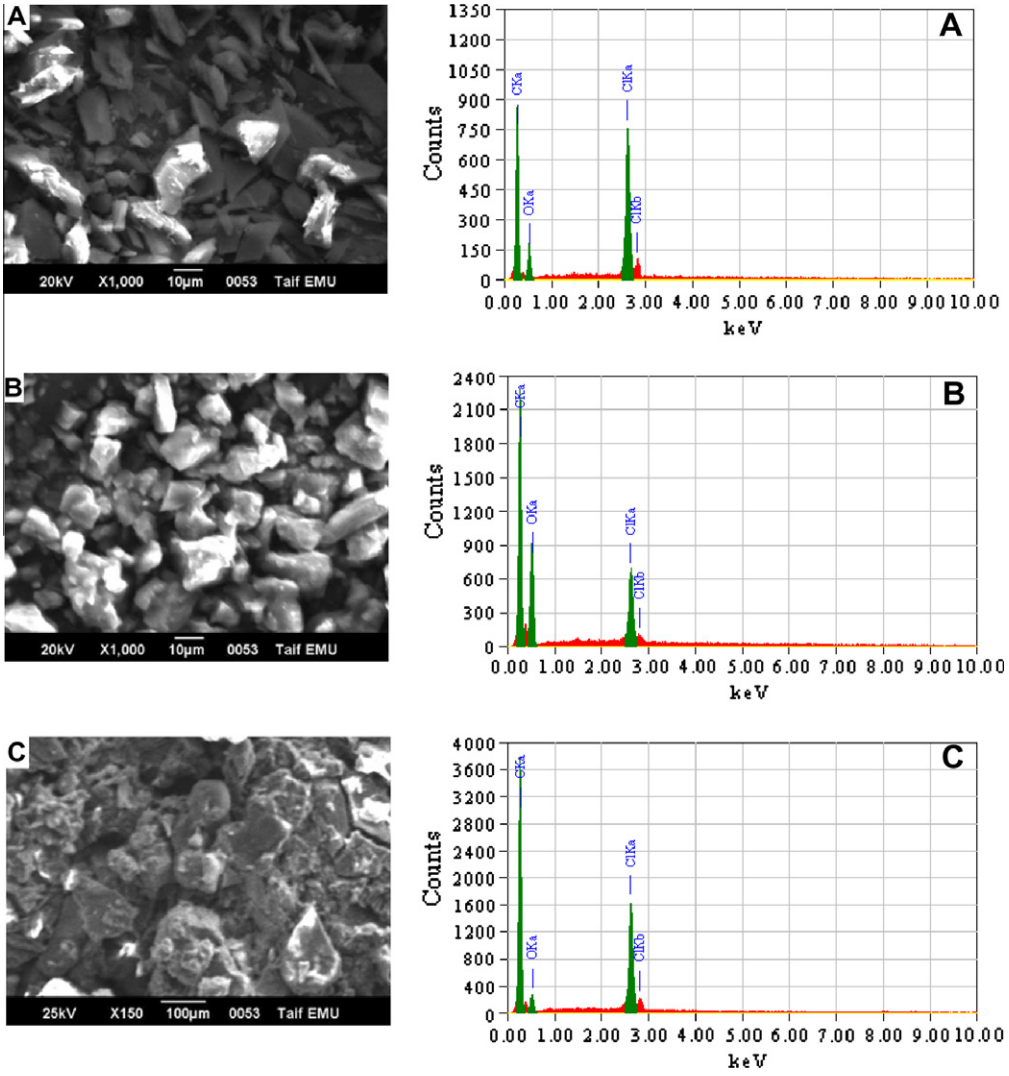


**Fig. 10.** SEM images and EDX spectra of (A) [(PC-HCl)(QL), (B) [(PC-HCl)(PA)] and [(PC-HCl)(TCNQ)] complexes.

elements are clearly identified, and the results confirm the proposed structures.

### 3.11. Antimicrobial activities

The antibacterial activity of newly synthesized CT complexes were tested in vitro against two Gram-positive bacteria strains, *Staphylococcus aureus* (*S. aureus*) and *B. subtilis*, and two Gram-negative bacteria strains, *Escherichia coli* (*E. coli*) and *Pseudomonas aeuroginosa* (*P. aeuroginosa*), using the disc diffusion method. Furthermore, the CT complexes were also screened for their antifungal properties against two species, *A. flavus* and *C. albicans*, in DMSO using the standard agar disc diffusion method. The activity was determined by measuring the inhibition zone diameter values (mm) of the investigated complexes against the microorganisms. Tetracycline was used as a standard drug for comparison of the

**Table 9**
The inhibition diameter zone values (mm) for PC-HCl CT-complexes.

| Sample | Inhibition zone diameter (mm/mg sample) | | | | | |
|---|---|---|---|---|---|---|
| | Bacteria | | | | Fungi | |
| | *Bacillus subtilis* ($G^+$)[a] | *Escherichia coli* ($G^-$) | *Pseudomonas aeuroginosa* ($G^-$) | *Staphylococcus aureus* ($G^+$) | *Aspergillus flavus* | *Candida albicans* |
| Control: DMSO | 0.0 | 0.0 | 0.0 | 0.0 | 0.0 | 0.0 |
| Standard | | | | | | |
| Tetracycline (Antibacterial agent) | 34.0 | 32.0 | 34.0 | 30.0 | – | – |
| Amphotericin B (antifungal agent) | – | – | – | – | 18.0 | 19.0 |
| PC-HCl/QL | 12.0 | 11.0 | 9.0 | 9.0 | 0.0 | 0.0 |
| PC-HCl/PA | 12.0 | 12.0 | 13.0 | 12.0 | 0.0 | 0.0 |
| PC-HCl/TCNQ | 0.0 | 11.0 | 0.0 | 0.0 | 0.0 | 0.0 |

[a] G: Gram reaction.

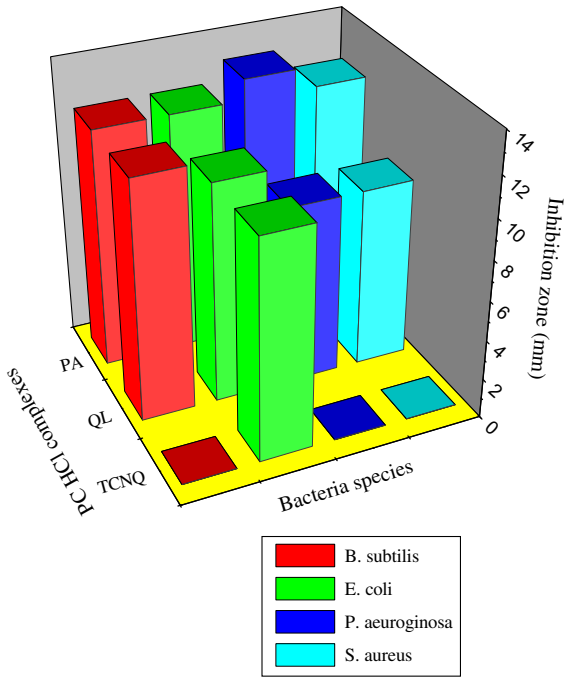


**Fig. 11.** Statistical representation for antibacterial activity of PC-HCl complexes.

bacterial results, whereas Amphotericin B was used as a standard drug for comparison of the antifungal results. The obtained screening results are listed in Table 9 and are statistically presented in Fig. 11. The results indicated that only the [(PC-HCl)(PA)] complex exhibits moderate antibacterial activity against the growth of the tested bacterial strains. The [(PC-HCl)(QL)] complex exhibits a moderate-to-weak antibacterial activity against all of the Gram-positive and Gram-negative bacteria species, whereas the [(PC-HCl)(TCNQ)] complex had no influence on the antibacterial profile of all of the tested strains (except *E. coli*). The data reveal that all of the three complexes exhibited no inhibitory activity against the fungi species.

## 4. Conclusions

Charge-transfer interactions between the drug procaine hydrochloride (PC-HCl) as a donor and quinol (QL), picric acid (PA) or 7,7′,8,8′-tetracyanoquinodimethane (TCNQ) as a π-acceptor were extensively studied in both solid and liquid phase at room temperature. It is observed that the reaction stoichiometry is 1:1, and the resulting CT complexes were shown to have the general formula: [(PC-HCl)(acceptor)]. The interaction between the donor and QL and PA acceptors was due to transfer of proton from acceptor to nitrogen atom of donor to make hydrogen bonding, where the interaction mode between PC-HCl and the TCNQ acceptor occurs through the migration of the $H^+$ ion from the $NH_2$ in the donor to one of the four cyano groups in the TCNQ acceptor to form a positive ion ($-C{\equiv}N^+H$) that associates with the anion to form ion pairs. The obtained complexes are semi-crystalline material and thermally stable. Physical parameters such as formation constant ($K_{CT}$), molar extinction coefficient ($\varepsilon_{CT}$) and other spectroscopic data and as well as the kinetic parameters ($E^*$, $A$, $\Delta S^*$, $\Delta H^*$ and $\Delta G^*$) have been estimated. Only the complex obtained using PA acceptor shows moderate antibacterial activity against various strains.

## References

[1] J. Yuan, J. Yin, E. Wang, J. Chromatogr., A 1154 (2007) 368.
[2] N. Li, Y. Chi, J. Wang, J. Duan, G. Chen, Luminescence 18 (2003) 125.
[3] Y. Chen, K. Lu, R. Hsiao, Y. Lee, H. Tsai, C.H. Lin, M. Tsai, J. Comp. Biochem. Physiol., C 148 (2008) 128.
[4] Ö. Karadaş, Ö.K. Omaç, F. Tok, A. Özgül, Z. Odabaşı, J. Neurol. Sci. 316 (2012) 76.
[5] Y. Liao, J. Chou, Mater. Chem. Phys. 114 (2009) 542.
[6] T. Roy, K. Dutta, M.K. Nayek, A.K. Mukherjee, M. Banerjee, B.K. Seal, J. Chem. Soc., Perkin Trans. 2 (1999) 531.
[7] F.P. Fla, J. Palou, R. Valero, C.D. Hall, P. Speers, J. Chem. Soc., Perkin Trans. 2 (1991) 1925.
[8] D.K. Roy, A. Saha, A.K. Mukherjee, Spectrochim. Acta A 61 (2005) 2017.
[9] A.M. Slifkin, Charge-Transfer Interaction of Biomolecules, Academic Press, New York, 1971.
[10] A. Dozal, H. Keyzer, H.K. Kim, W.W. Wang, Int. J. Antimicrob. Agent 14 (2000) 261.
[11] A. Korolkovas, Essentials of Medical Chemistry, second ed., Wiley, New York, 1998 (Chapter 3).
[12] F.M. Abou Attia, Il Farmaco 55 (2000) 659.
[13] K. Basavaiah, Il Farmaco 59 (2004) 315–321.
[14] G.A. Saleh, H.F. Askal, M.F. Radwan, M.A. Omar, Talanta 54 (2001) 1205.
[15] H. Salem, J. Pharm. Biomed. Anal. 29 (2002) 527.
[16] M. Pandeeswaran, E.H. El-Mossalamy, K.P. Elango, Int. J. Chem. Kinet. 41 (2009) 787.
[17] M. Pandeeswaran, K.P. Elango, Spectrochim. Acta A 75 (2010) 1462.
[18] F. Yakuphanoglu, M. Arslan, Solid State Commun. 132 (2004) 229.
[19] F. Yakuphanoglu, M. Arslan, Opt. Mater. 27 (2004) 29.
[20] F. Yakuphanoglu, M. Arslan, M. Kucukislamoglu, M. Zengin, Sol. Energy 79 (2005) 96.
[21] B. Chakraborty, A.S. Mukherjee, B.K. Seal, Spectrochim. Acta A 57 (2001) 223.
[22] M. Krishnamurthy, K. Surendrababu, U. Muralikrishna, Indian J. Chem. 27A (1988) 669.
[23] S.M. Andrade, S.M.B. Costa, R. Pansu, J. Colloid Interface Sci. 226 (2000) 260.
[24] R. Dabestani, K.J. Reszka, M.E. Sigman, J. Photochem. Photobiol., A 117 (1998) 223.
[25] R. Jakubiak, Z. Bao, L. Rothberg, Synth. Met. 114 (2000) 61.
[26] K. Takahasi, K. Horino, T. Komura, K. Murata, Bull. Chem. Soc. Jpn. 66 (1993) 733.
[27] A. Eychmuller, A.L. Rogach, Pure Appl. Chem. 72 (2000) 179.
[28] K. Brueggermann, R.S. Czernuszewicz, J.K. Kochi, J. Phys. Chem. 96 (1992) 4405.
[29] S.K. Das, G. Krishnamoorthy, S.K. Dofra, Can. J. Chem. 78 (2000) 191.
[30] G. Jones, J.A.C. Jimenez, Tetrahedron Lett. 40 (1999) 8551.
[31] G. Smith, D.E. Lynch, K.A. Byriel, C.H.L. Kennard, J. Chem. Crystallogr. 27 (1997) 307.
[32] G. Smith, D.E. Lynch, R.C. Bott, Aust. J. Chem. 51 (1998) 159.
[33] G. Smith, R.C. Bott, A.D. Rae, A.C. Willis, Aust. J. Chem. 53 (2000) 531.
[34] D.A. Skoog, Principle of Instrumental Analysis, third ed., Saunders, New York, USA, 1985 (Chapter 7).
[35] H.A. Benesi, J.H. Hildebrand, J. Am. Chem. Soc. 71 (1949) 2703.
[36] R. Abu-Eittah, F. Al-Sugeir, Can. J. Chem. 54 (1976) 3705.
[37] A.W. Bauer, W.M. Kirby, C. Sherris, M. Turck, Am. J. Clin. Pathol. 45 (1966) 493.
[38] M.A. Pfaller, L. Burmeister, M.A. Bartlett, M.G. Rinaldi, J. Clin. Microbiol. 26 (1988) 1437.
[39] D.J. Beecher, A.C. Wong, Appl. Environ. Microbiol. 60 (1994) 1646.
[40] National Committee for Clinical Laboratory Standards, Reference Method for Broth Dilution Antifungal Susceptibility Testing of Conidium-Forming Filamentous Fungi: Proposed Standard M38-A, NCCLS, Wayne, PA, USA, 2002.
[41] National Committee for Clinical Laboratory Standards, Method for Antifungal Disk Diffusion Susceptibility Testing of Yeast: Proposed Guideline M44-P, NCCLS, Wayne, PA, USA, 2003.
[42] National Committee for Clinical Laboratory Standards, Methods for Antimicrobial Susceptibility Testing of Anaerobic Bacteria: Approved Standard M11-A3, NCCLS, Wayne, PA, USA, 1993.
[43] H. Tsubomura, R.P. Lang, J. Am. Chem. Soc. 83 (1961) 2085.
[44] R. Rathone, S.V. Lindeman, J.K. Kochi, J. Am. Chem. Soc. 119 (1997).
[45] G. Aloisi, S. Pignataro, J. Chem. Soc., Faraday Trans. 69 (1972) 534.
[46] G. Briegleb, J. Czekalla, Z. Physikchem, Frankfurt 24 (1960) 237.
[47] G. Briegleb, Z. Angew. Chem. 72 (1960) 401;
G. Briegleb, Z. Angew. Chem. 76 (1964) 326.
[48] A.N. Martin, J. Swarbrick, A. Cammarata, Physical Pharmacy, third ed., Lee and Febiger, Philadelphia, PA, 1969. p. 344.
[49] M.S. Refat, A. Elfalaky, E. Elesh, J. Mol. Struct. 990 (2011) 217.
[50] M. Pandeeswaran, K.P. Elango, Spectrochim. Acta A 65 (2006) 1148.
[51] M.S. Refat, L.A. El-Zayat, O.Z. Yeşilel, Spectrochim. Acta A 75 (2010) 745.
[52] M.S. Refat, H.A. Saad, A.A. Adam, J. Mol. Struct. 995 (2011) 116.
[53] L.J. Bellamy, The Infrared Spectra of Complex Molecules, Chapman & Hall, London, 1975.
[54] R. Bharathikannan, A. Chandramohan, M.A. Kandhaswamy, J. Chandrasekaran, R. Renganathan, V. Kandavelu, Cryst. Res. Technol. 43 (6) (2008) 683.
[55] R.D. Kross, V.A. Fassel, J. Am. Chem. Soc. 79 (1957) 38.
[56] M.S. Refat, J. Mol. Struct. 985 (2011) 380.
[57] G.G. Mohamed, Shaban M. Khalil, M.A. Zayed, M. Abd El-Hamid El-Shall, J. Pharm. Biomed. Anal. 28 (2002) 1127.
[58] A.S. Amine, M.E. Moustafa, Y.M. Issa, Microchem. J. 50 (1994) 6.
[59] M.S. Refat, H.A. Saad, A.A. Adam, Spectrochim. Acta A 79 (2011) 672.
[60] A.W. Coats, J.P. Redfern, Nature (London) 201 (1964) 68.
[61] H.H. Horowitz, G. Metzger, Anal. Chem. 35 (1963) 1464.
[62] S.J.S. Qazi, A.R. Rennie, J.K. Cockcroft, M. Vickers, J. Colloid Interface Sci. 338 (2009) 105.